FYSC23

Powder X-ray Diffraction Lab

Authors
Fredrik Bergelv
Max Eriksson
fredrik.bergelv@live.se
maxerikss@gmail.com

LUND UNIVERSITY

March 11, 2025

Abstract

Determining the structure of crystals is of the utmost importance for understanding the properties of a material, with applications in material science, electronics, and even medicine. This report uses the method of powder X-ray diffraction (PXRD) to analyze two unknown samples. Using the angle peaks from the detector and comparing these with tabulated values, the first sample was identified to be gold (Au), and the second one to be iron (Fe). Analysis using Scherrer's equation yielded the mean particle size for the gold powder to be approximately 13.44 nm and 11.2 nm for the iron powder. The results aligned with tabulated values, validating the method despite minor deviations attributed to instrumental uncertainties.

Contents

1 Introduction

Determining the crystal structure of materials is important to understand how these materials behave, a crucial part for developing e.g. medicine, and electronics. Common ways to analyse crystal structure is diffraction experiments, where X-ray diffraction is especially well suited because of the small wavelength on the order of the lattice parameters. The experiment conducted in this report specifically uses a type of X-ray diffraction called powder X-ray diffraction. The goal of this report is to determine the structure and size of to unknown samples.

2 Theory

2.1 Crystal Lattice Structure

Crystal lattice structures are described by a Bravais lattice [1] which is an infinite array of points described by translational operations

$$\mathbf{R} = n_1\mathbf{a}_1 + n_2\mathbf{a}_2 + n_3\mathbf{a}_3, \tag{1}$$

where $\mathbf{a}_i$ are the lattice vectors. Performing a Fourier transform of the real space lattice gives the reciprocal lattice in k-space, also a Bravais lattice, which is described by the reciprocal lattice vectors $\mathbf{b}_j$ defined by $\mathbf{a}_i \cdot \mathbf{b_j} = 2\pi\delta_{ij}$ [1]. The reciprocal lattice is useful when performing diffraction experiments since the diffraction pattern is in k-space.

To calculate the distance between planes the formula

$$\frac{1}{d^2} = \frac{h^2}{a^2} + \frac{k^2}{b^2} + \frac{l^2}{c^2} \tag{2}$$

is used. If we use this formula for a simple cubic with $a = b = c = 4.32 \times 10^{-1}$ nm for the plane(111) we get the separation to $d = 2.49 \times 10^{-1}$ nm. If we do the same for the plane (211) we obtain a separation of $d = 1.76 \times 10^{-1}$ nm and for the plane (100) we get $d = 4.32 \times 10^{-1}$ nm.

2.2 Diffraction

Diffraction is when light passes an obstacle, like an aperture, and the light deviates and spreads out [1]. In scattering experiments constructive and destructive interference can be observed which forms diffraction patterns that is analysed. Depending on the size of the obstacle, the wavelength of the light need to be chosen accordingly. For example, to resolve atomic structure the wavelength need to be on the same order as the lattice spacing, which is X-rays [1].

To evaluate diffraction patterns Bragg's law is mainly used, with is defined as

$$n\lambda = 2d\sin\theta, \tag{3}$$

where n is an integer, λ is the wavelength of the incoming photon, d is the spacing between the planes and θ is the scattering angle. Using this we see that if the incoming x-ray has a wavelength of 7×10^{-2} nm we can at minimum spacing which can be observed is 3.5×10^{-1} Å. In order to observe smaller spacings, a higher photon energy would have to be used.

For example if we have a (111) plane with an incident angle $\theta = 11.2°$ when X-rays of wavelength of 0.154 nm then the side of the side of each unit cell can be calculated as follows: From Equation 3 we obtain a the distance planer separation to $d = 3.97 \times 10^{-1}$ nm, from Equation 2 we obtain that a separation of $d = 3.97 \times 10^{-1}$ nm leads to a lattice constant of $a = 6.36$ Å for a simple cubic.

Another example for a orthorhombic unit cell with dimensions $a = 5.74$ Å, $b = 7.96$ Å and $c = 4.95$ Å one can calculate the incident angles for the (100), (010), and (111) planes if the wavelength is 8.3×10^{-2} nm. For the (100) plane Equation 2 gives a planar separation of $d_{(100)} = 5.74 \times 10^{-1}$ nm, (010) gives $d_{(010)} = 7.96 \times 10^{-1}$ nm and (111) gives $d_{(111)} = 3.39 \times 10^{-1}$ nm. Using Equation 3 the following angles are found: $\theta_{(100)} = 4.15°$, $\theta_{(010)} = 2.99°$ and $\theta_{(111)} = 7.03°$.

From Equation 3 we can derive the following:

$$\frac{d}{d\lambda}(n\lambda) = \frac{d}{d\lambda}(2d\sin\theta) \implies n = 2d\cos\theta\frac{d\theta}{d\lambda} = 2d\cos\theta\frac{\Delta\theta}{\Delta\lambda}, \tag{4}$$

using Bragg's law once again we obtain

$$\implies \frac{2d\sin\theta}{\lambda} = 2d\cos\theta\frac{\Delta\theta}{\Delta\lambda} \implies \Delta\theta = \frac{\Delta\lambda}{\lambda}\tan\theta. \tag{5}$$

This relation shows that the spectral contribution to the peak width θ is related to the spectral bandwidth $\Delta\lambda/\lambda$. However one must note that the broadening is also affected by other factors.

2.3 Structure Factors

Due to the structure of different types of lattices, the diffraction pattern may change. This is due to structure function which are defined as

$$F(hkl) = \sum_m f_m \exp\left(2\pi i(u_m h + v_m k + w_m l)\right). \tag{6}$$

where f_m is the atomic form factor and (u_m, v_m, w_m) are the fractional coordinates of atoms in the unit cell. for a BCC we know that we have the fractional coordinates (0,0,0) for each corner and (1/2,1/2,1/2). and for an FCC we have the (0,0,0) for each corner, (0,1/2,1/2), (1/2,0,1/2) and (1/2,1/2,0). In the equation above h,k,l is the value of the miller index. Putting all of this together we know that we will obtain diffraction peaks only if $F(hkl) \neq 0$ [2].

From this we can evaluate which planes we will see from BCC and FCC. From Equation 6 we can see that the points located at (0,0,0) will always yield a non-zero result. However, if we start looking at the BCC crystal we can obtain the following:

$$F(hkl) = f_m \exp\left[2\pi i\,(0h + 0k + 0l)\right] + f_m \exp\left[2\pi i\left(\frac{h}{2} + \frac{k}{2} + \frac{l}{2}\right)\right] = f_m\left[1 + \exp\left(2\pi i\frac{h+k+l}{2}\right)\right] \tag{7}$$

$$\text{if } F(hkl) \neq 0 \implies -1 \neq \exp\left(2\pi i\frac{h+k+l}{2}\right) \implies \frac{h+k+l}{2} \neq n + \frac{1}{2}, \text{ where n=1,2,3...} \tag{8}$$

$$\implies h + k + l \neq 2n + 1. \tag{9}$$

Above we used Euler's identity which says $\exp(i\pi(n + 1/2) + 1 = 0$. We have thus shown that for the BCC structure wont show any planes where $h + k + l$ are odd. For the FCC we get the following instead:

$$F(hkl) = f_m + f_m \exp\left[2\pi i\left(\frac{h}{2} + \frac{k}{2}\right)\right] + f_m \exp\left[2\pi i\left(\frac{h}{2} + \frac{l}{2}\right)\right] + f_m \exp\left[2\pi i\left(\frac{k}{2} + \frac{l}{2}\right)\right] \tag{10}$$

$$\text{if } F(hkl) \neq 0 \implies -1 \neq \exp\left[2\pi i\left(\frac{h}{2} + \frac{k}{2}\right)\right] + \exp\left[2\pi i\left(\frac{h}{2} + \frac{l}{2}\right)\right] + \exp\left[2\pi i\left(\frac{k}{2} + \frac{l}{2}\right)\right] \tag{11}$$

As shown before, we can see above if one of h, k, l is even and the other are odd (or vice versa) then we get $-1 \neq 1 - 1 - 1$ which is not allowed. However if all h, k, l are even or odd we obtain $-1 \neq 1 + 1 + 1$ which is true. Thus the (h,k,l) is always all odd or all even for the FCC.

The order of the peaks we will see will be ordered as

$$\sqrt{h^2 + k^2 + l^2}, \tag{12}$$

where h, k and l are the miller indices of that specific plane. Thus, for a BCC crystal the peaks will be in the order (110), (200), (211), (220) and so on. For the FCC the peaks will be (111), (200), (220), (311), (222) and so on.

2.4 Powder X-ray Diffraction

Powder X-ray diffraction (PXRD) is a method of diffraction to analyse crystal structure. In PXRD the sample is a fine powder of many small crystallites instead of a single large crystal [1]. This means that the crystal planes will be randomly oriented, and all possible orientations will be present. The diffraction pattern will look like a series of rings, instead of sharp points which arises from single crystal diffraction [1]. One of the advantages of powder diffraction is that it is quicker than other methods of analysing crystal structures.

Scherrer's formula is used to estimate the size of crystallites based on the broadening of diffraction peaks as

$$t = \frac{k\lambda}{\beta \cos\theta}, \tag{13}$$

where t is the size of the crystallites, λ is the wavelength of the x-ray, k is the shape factor which varies with the full width half maximum β but the value 0.94 is used here [2]. However, one must note that the Scherrer's equation is accurate for crystallites smaller than 100 nm, as larger particles lead to much narrower peaks where factors, such as instrumental broadening, become more influential. To obtain the full width at half maximum the equation

$$\beta = 2\sqrt{2\ln(2)}\sigma, \tag{14}$$

where σ is the standard deviation.

3 Method

The experimental setup consisted of an X-ray source pointing on a sample of powdered crystal. The sample was placed on a diffractometer connected to a computer to control the placement of the sample. Behind the sample was a large area detector used to capture the diffraction rings. The setup can bee seen in 1

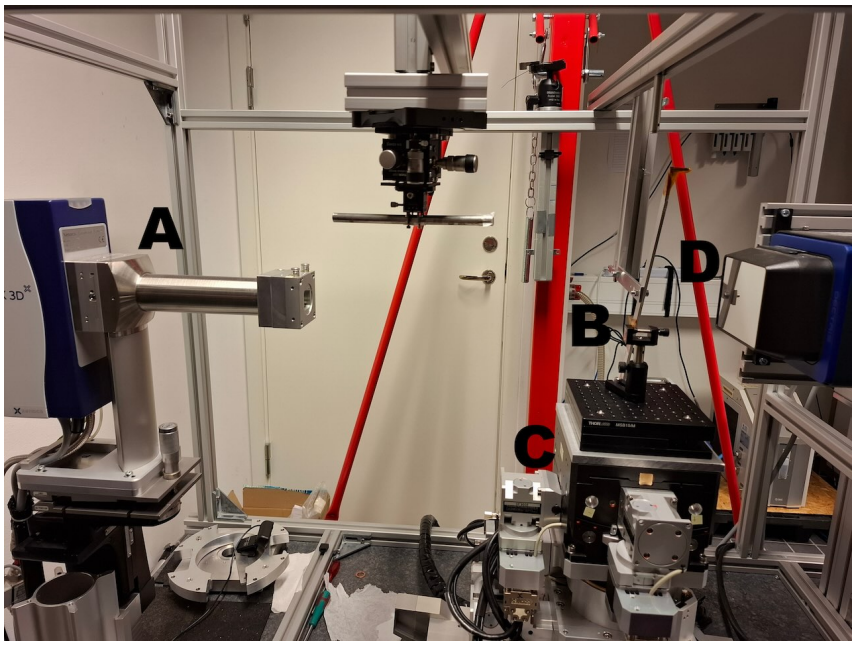

Figure 1: The experimental setup. **A** is the X-ray source with X-ray energy of 1.745×10^1 keV. **B** is the sample which were analysed. In the lab two different samples were tested. **C** is the diffractometer used to control the position of the sample. **D** is the detector made from six large semiconductors.

During the lab the powders sample was put on the diffractometer, then the shutter on the X-ray source was opened, and the detector started recording. The diffractometer was controlled from the computer to move the sample until a diffraction pattern was seen in the detector. A 1-minute-long measurement were taken and the data saved. The process was repeated for the other sample as well.

Before analysing the data, the data was calibrated using the calibration sample LaB_6. The rings from the calibration sample were marked to calibrate the detector. During the analysis the data was masked to remove parts of the dead spots on the detector and hot spots where the detector was saturated. Then a 1D plot was generated from the 2D image to show the intensity as a function of the scattering angle. In some cases there were so called hot pixels, which are high peak intensities with no width. This is probably due to a pixel being burnt out, and these points were removed from the data.

4 Result

In Figure 2 one can see the given spectrum together with gaussian fits of all the peaks. The extracted mean peak angle, the standard deviation and the calculated full with maxima (using Equation 14) can bee seen in Table 1 and Table 2.

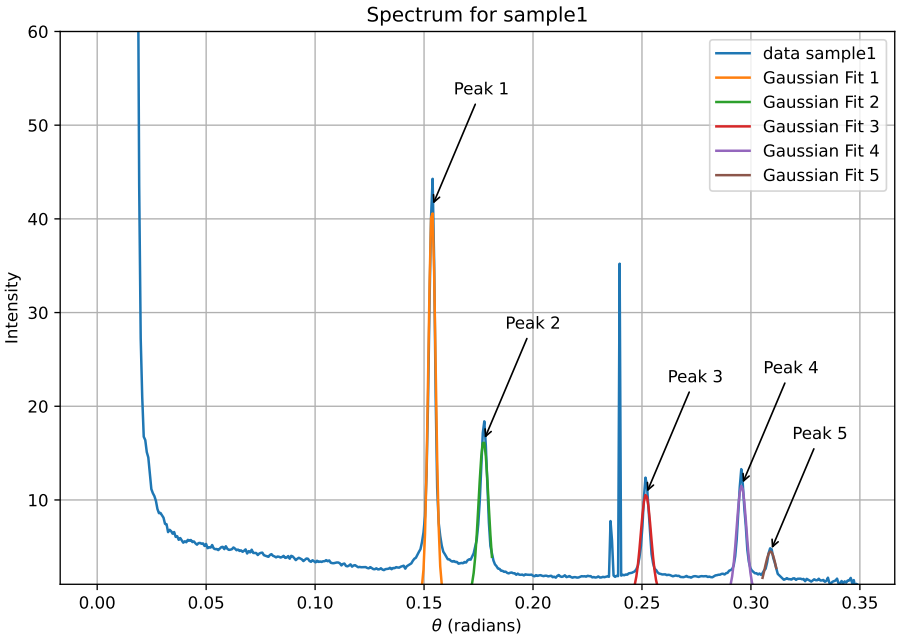

(a) This is the spectrum from sample 1.

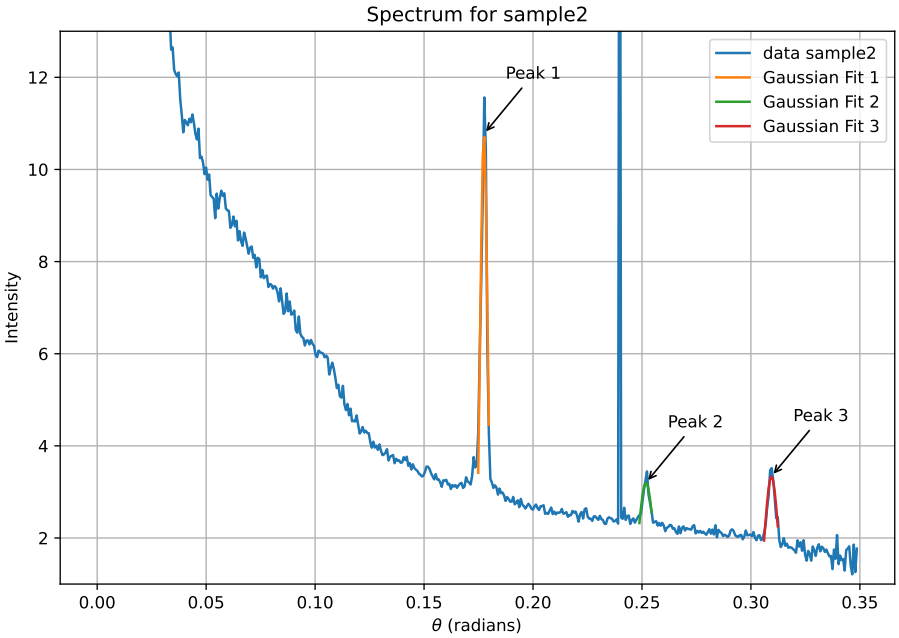

(b) This is the spectrum from sample 2.

Figure 2: These plots display the spectrum gathered from the detector. It is evident that the sharp peaks in both plots are caused by hot pixels, damaged detector elements that produce spurious signals.

Table 1: Fitting results for Sample 1

Peak	Angle θ (radians)	Standard deviation σ (radians)	FWHM (radians)
Peak 1	$(1.5362 \pm 0.0010) \times 10^{-1}$	$(1.65 \pm 0.10) \times 10^{-3}$	$(3.88 \pm 0.23) \times 10^{-3}$
Peak 2	$(1.7731 \pm 0.0019) \times 10^{-1}$	$(2.27 \pm 0.20) \times 10^{-3}$	$(5.35 \pm 0.46) \times 10^{-3}$
Peak 3	$(2.5180 \pm 0.0018) \times 10^{-1}$	$(2.34 \pm 0.18) \times 10^{-3}$	$(5.50 \pm 0.43) \times 10^{-3}$
Peak 4	$(2.9569 \pm 0.0015) \times 10^{-1}$	$(2.25 \pm 0.15) \times 10^{-3}$	$(5.30 \pm 0.35) \times 10^{-3}$
Peak 5	$(3.0900 \pm 0.0015) \times 10^{-1}$	$(2.61 \pm 0.21) \times 10^{-3}$	$(6.16 \pm 0.49) \times 10^{-3}$

Table 2: Fitting results for Sample 2

Peak	Angle θ (radians)	Standard deviation σ (radians)	FWHM (radians)
Peak 1	$(1.7746 \pm 0.0012) \times 10^{-1}$	$(1.72 \pm 0.14) \times 10^{-3}$	$(4.04 \pm 0.34) \times 10^{-3}$
Peak 2	$(2.5186 \pm 0.0017) \times 10^{-1}$	$(3.80 \pm 0.39) \times 10^{-3}$	$(8.95 \pm 0.92) \times 10^{-3}$
Peak 3	$(3.0942 \pm 0.0014) \times 10^{-1}$	$(3.26 \pm 0.24) \times 10^{-3}$	$(7.68 \pm 0.56) \times 10^{-3}$

Using peak 1 from the first sample and $n = 1$, the plane (111) we obtain a spacing $a = (4.0213 \pm 0.0026)$ Å which coincides with the material Au, with $a = 4.065$ Å, using Equation 3 and Equation 2 with the given table [2]. The first peak coincides with the plane (111) as seen in Equation 12 and all indices are odd which is must be true since Au is a FCC. This verifies this result.

Using peak 2 from the second sample and $n = 1$, the plane (110) we obtain a spacing $a = (2.8484 \pm 0.0030)$ Å which coincides with the material Fe, with $a = 2.856$ Å, using Equation 3 and Equation 2 with the given table [2]. The second peak coincides with the plane (110) as seen in Equation 12, also the sum of the miller indices is even which must be true for a BCC such as Fe, verifying this result.

Using Equation 13, we obtain the following particle sizes as shown in Table 3 and Table 4. The mean particle size for Sample 1 is (13.44 ± 0.04) nm, and for Sample 2, it is (11.2 ± 0.6) nm.

Table 3: Powder size t for Sample 1

Peak	Size (m)
Peak 1	$(1.74 \pm 0.10) \times 10^{-7}$
Peak 2	$(1.27 \pm 0.11) \times 10^{-7}$
Peak 3	$(1.25 \pm 0.10) \times 10^{-7}$
Peak 4	$(1.32 \pm 0.09) \times 10^{-7}$
Peak 5	$(1.14 \pm 0.09) \times 10^{-7}$

Table 4: Powder size t for Sample 2

Peak	Size (m)
Peak 1	$(1.68 \pm 0.14) \times 10^{-8}$
Peak 2	$(7.7 \pm 0.8) \times 10^{-9}$
Peak 3	$(9.1 \pm 0.7) \times 10^{-9}$

5 Discussion

The uncertainties of the Gaussian fit can be seen in Table 1 and Table 2. We can see that the calculated lattice constant for Sample 1, which is made of gold, includes the tabulated value within its uncertainty. However, this is not true for the second sample, made of iron. The calculated lattice constant for Sample 2 deviates by only 1% from the tabulated value. Thus, one can argue that this is close enough for us to validate the result. The small deviation in Sample 2 might be due to other errors that have not been accounted for, such as errors in the X-ray energy and measurement equipment. Errors such as beam divergence, finite spectral bandwidth, and detector resolution also contribute to uncertainties.

In Figure 2, we can identify the peaks using the theory derived above. Since we know that Sample 1 was gold, which has an FCC structure, the first peak corresponds to the (111) plane, the second peak to the (200) plane, the third peak to the (220) plane, the fourth peak to the (331) plane, and the fifth peak to the (222) plane. For the second sample, we know that the material was iron with a BCC structure. This means that the first peak corresponds to the (110) plane, the second peak to the (200) plane, and the third peak to the (211) plane.

The mean size of the gold and Fe powders also seems plausible. It is interesting to note that the iron powder was smaller than the gold powder. Both of these values, however, fall within a reasonable range for powder materials. There was also some variation in the powder size, which is expected since not all particles are exactly the same size.

In Equation 5, it was shown that the spectral contribution of the X-ray source to the peak width was related to the spectral bandwidth. However, other factors also contribute to instrumental broadening, such as the width of the X-ray beam, beam divergence, and the resolution of the detector. Additional broadening effects arise due to disorder of the second kind, where atomic fluctuations cause variations in the distances between neighboring atoms. This leads to peak broadening and a decrease in peak height [3]. This effect becomes more pronounced at increasing angles, meaning that it has a greater impact on higher-order peaks.

6 Conclusion

In this lab, X-ray powder diffraction (PXRD) was used to analyze the crystal structures of two unknown samples. By applying Bragg's law and structure factor analysis, Sample 1 was identified as gold (Au) with an FCC structure, while Sample 2 was identified as iron (Fe) with a BCC structure. The calculated lattice parameter for Sample 1 matched tabulated values exactly, whereas Sample 2 showed a close match with minor deviations, likely due to experimental uncertainties such as instrumental broadening, beam divergence, and spectral bandwidth limitations. Additionally, the Scherrer equation was used to estimate the crystallite size of both samples, yielding values in the range of a couple of nanometers for the gold powder and a couple nanometers for the iron powder. Overall, the results demonstrated the effectiveness of PXRD in identifying material types and determining their crystalline structures.

References

[1] Philip Hofmann. *Solid State Physics: An Introduction*. Wiley-VCH, 2nd edition, 2015.

[2] Auden Ti and Hajar Jalili. *FYSC23: Powder X-ray Diffraction Laboratory Manual*. Lund, 2025. Lab instructors: Auden Ti (`auden.ti_yun@sljus.lu.se`) and Hajar Jalili (`hajar.jalili@sljus.lu.se`).

[3] A. Guinier. *X-Ray Diffraction*. WH Freeman, San Francisco and London, 1963.